Journal of Marine Science and Technology

Volume 25 | Issue 5 Article 5

NUMERICAL SIMULATIONS OF WATER SURFACE PROFILES AND VORTEX STRUCTURE IN A VORTEX SETTLING BASIN BY USING FLOW-3D

Tsung-Hsien Huang
Department of Hydraulic & Ocean Engineering, National Cheng Kung University, Taiwan, R.O.C.

Chyan-Deng Jan
Department of Hydraulic & Ocean Engineering, National Cheng Kung University, Taiwan, R.O.C.,
cdjan@mail.ncku.edu.tw

Yu-Chao Hsu
Department of Hydraulic & Ocean Engineering, National Cheng Kung University, Taiwan, R.O.C.

Recommended Citation
Huang, Tsung-Hsien; Jan, Chyan-Deng; and Hsu, Yu-Chao (2017) "NUMERICAL SIMULATIONS OF WATER SURFACE PROFILES AND VORTEX STRUCTURE IN A VORTEX SETTLING BASIN BY USING FLOW-3D," *Journal of Marine Science and Technology*: Vol. 25: Iss. 5, Article 5.
DOI: 10.6119/JMST-017-0509-1
Available at: https://jmstt.ntou.edu.tw/journal/vol25/iss5/5

Journal of Marine Science and Technology, Vol. 25, No. 5, pp. 531-542 (2017)
DOI: 10.6119/JMST-017-0509-1

NUMERICAL SIMULATIONS OF WATER SURFACE PROFILES AND VORTEX STRUCTURE IN A VORTEX SETTLING BASIN BY USING FLOW-3D

Tsung-Hsien Huang, Chyan-Deng Jan, and Yu-Chao Hsu

Key words: vortex settling basin, vortex flow, air core, FLOW-3D.

ABSTRACT

A vortex settling basin (VSB), consisting of a cylindrical chamber, an inflow system, a bottom orifice outflow and an overflow weir, has been used to separate sediment from sediment-laden water flow. The efficiency of sediment extraction by a VSB is significantly dependent on the flow characteristics of the device. The vortex in a VSB is complex and it is very difficult if not impossible to measure it by using a direct measurement. The VSB used in this study has a cylinder of 100 cm in diameter and 30 cm in height, with an overflow weir 15 cm height above the bottom. This study numerically assessed the velocity distribution in the VSB by using FLOW-3D. Comparison of the water surface profiles obtained from experiments and simulations shows that the simulated results are quite close to the experimental results, and this indicates that FLOW-3D is a suitable software for simulating flow field in a VSB. The comparisons between inflow depth and outflow discharges indicate there is less than 3.46% error between the numerical output and experimental data. Simulated velocity distributions at the depths of 6.3 cm (the distance from the bottom), 10.3 cm, and 14.3 cm (near the surface layer) were analyzed, respectively. The characteristics of velocity components (tangential, radial, and axial velocities) at these three depths were considered, in addition to the velocity distributions, the formation of an air core in the central part of vortex flow was also simulated and considered. Both the experimental and numerical results show the existence of air core oscillation. The oscillation may cause some changes in the flow field, especially in the high velocity zone, but the overall change in the whole flow field is not obvious.

I. INTRODUCTION

A vortex settling basin (VSB) is a fluidic device which is used to extract bed load and suspended load sediment from the diverted water by the vortices of flow (Paul et al., 1991). A tangential inflow is introduced into a cylindrical chamber with a bottom orifice; thus, a strong vortex flow is produced there. Under the action of gravity and centrifugal force, heavier sediment particles are forced to move towards the bottom orifice, and relatively clear water flows over through the top overflow weir. There are three basic approaches that could be used to understand the flow in a VSB, which include efficiency experiments, measuring instruments and numerical simulations. The majority of previous investigators have focused on the sediment removal efficiency and water loss rate in a VSB (Cecen and Akmandor, 1973; Mashauri, 1986; Paul et al., 1991; Athar et al., 2002; Keshavarzi and Gheisi, 2006; Niknia et al., 2011; Hsu et al., 2013; Hajiahmadi et al., 2014; Jan et al., 2014). The sediment removal efficiency of a VSB significantly depends on the flow characteristics in the VSB.

To date, many experimental studies have been conducted to investigate velocity components inside a VSB. Hite et al. (1994) used the two-component laser doppler anemometer to measure the tangential velocity within the device; however, he found that this methodology was impossible to complete the velocity measurement because of the instability of vortex flow. The EMV-89 electromagnetic velocity meter was ever employed by Wang et al. (2002) to investigate vertical, radial and tangential velocity components in a VSB. Noguchi et al. (2003) used the device of a particle image velocimetry (PIV) to measure the velocity distribution, and found that the PIV could not complete the measurement of the velocity component in the vertical direction. Chapokpour and Farhoudi (2011) used an acoustic doppler velocity (ADV) meter to measure the flow field inside a VSB, and found that the results obtained from the experiments were not accurate enough because the ADV device significantly disturbed the flow within the VSB. They noticed that the measurement on the velocity field inside a VSB using experimental devices can provide only an initial understanding of flow characteristics. A suitable numerical model is useful to simulate the flow field in a VSB. In the past considerable attention has been given to the flow characteristics in a VSB, but the development of numerical approaches is relatively slow.

Ziaei and McDonough (2007) numerically simulated the flow

Paper submitted 11/27/16; revised 03/24/17; accepted 05/09/17. Author for correspondence: Chyan-Deng Jan (e-mail: cdjan@mail.ncku.edu.tw).
Department of Hydraulic & Ocean Engineering, National Cheng Kung University, Taiwan, R.O.C.

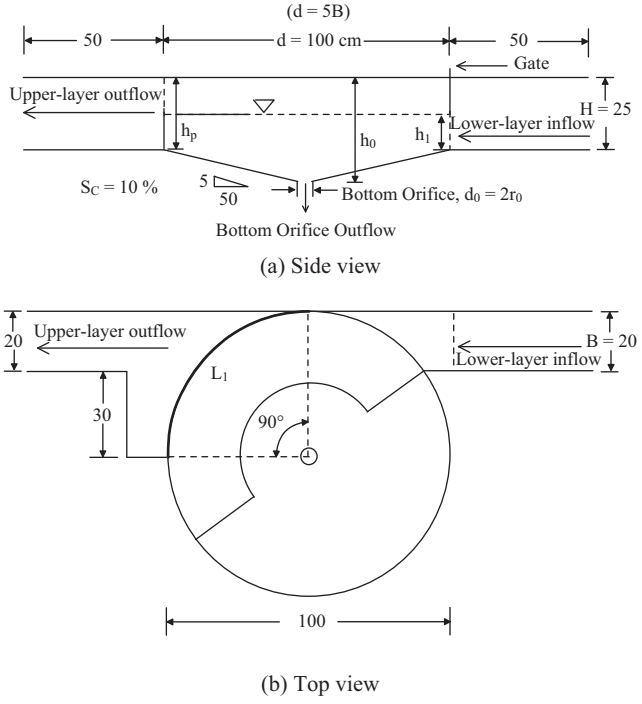

Fig. 1. Schematic diagram of a vortex settling basin.

in a vortex settling basin with multiple open boundaries by k-ε and k-ω turbulence models, and suggested that the numerical results needed to be calibrated with the experimental data. The numerical model FLOW 3D was used by Chapokpour et al. (2012) to simulate the vortex behavior within a vortex chamber. In general, a lot of data have been obtained from experimental studies and numerical models, but little has been done with the calibration of experimental results.

Because the vortex flow in a VSB is very complex, and it is very difficult if not impossible to measure it by a direct measurement, a suitable numerical approach is needed to obtain the vortex-flow characteristics. The present study is intended to apply an efficiency numerical model to obtain better flow data in a VSB, such as the water surface profile, the discharge load, the flow field structure, and the air core forming process. Some numerical results are also compared with those obtained from laboratory experiments.

II. LABORATORY EXPERIMENT

The experimental VSB setup used for this study was on the basis of the guidelines provided by Athar et al. (2002), with a cylinder of 100 cm in diameter and 30 cm in height. The elevation of the overflow weir is 15 cm from the bottom of the cylinder, and the width of the overflow weir is one quarter of the cylinder circumference, as shown in Fig. 1. The orifice located at the center of the bottom is 3 cm in diameter. The inflow channel is 50 cm long, 20 cm wide and 25 cm high. The inflow enters the cylinder in the form of the culvert at the connecting position. The main parts of the VSB were made of transparent acrylic material. Additionally, a recycle water system was made of stainless steel to connect the inflow channel and the outflow tank of the VSB. The basic component parts of the VSB used herein contain a vortex chamber (water tank), a recycle tank, a pump and two settling tanks for collecting the flows and sediments coming from the bottom orifice and the overflow weir.

Table 1. Inflow conditions for experiments and numerical simulations.

Case	Channel width B (cm)	Flow depth h (cm)	Average velocity V_c (cm/s)	Inflow Discharge Q_{cc} (cms)
# 1	20.0	16.88	22.5	1.5×10^{-3}
# 2	20.0	16.98	27.0	2.0×10^{-3}
# 3	20.0	17.15	30.8	2.5×10^{-3}
# 4	20.0	17.69	35.5	4.0×10^{-3}

In the design of the VSB model used herein, most structural items are replaceable, including all adjustable orifices, overflow weirs, horizontal deflectors, bottom slope, inflow and outflow direction. In this study, we kept the structures the same, except the inflow discharge.

The inflow discharges used in this study were $Q_{cc} = 1.5 \times 10^{-3}$ cms, 2.0×10^{-3} cms, 2.5×10^{-3} and 4.0×10^{-3} cms, respectively, and the corresponding heights of water surface (h) were 16.88 cm, 16.98 cm, 17.15 cm and 17.69 cm, respectively. All the inflow conditions are listed in Table 1. The conditions listed in the table were used in both laboratory and numerical simulations. The water surface profile and the discharge data obtained from experiments are used to compare with the results from numerical simulations.

III. NUMERICAL SIMULATION

By using the commercial software FLOW-3D, this study tries to numerically assess the velocity distribution in the VSB. The model used for numerical simulations and experiments in this study are in one to one structure scale. As shown in Fig. 2, we utilized two rectangular blocks, Block 1 (the cylinder chamber) and Block 2 (the inlet), to setup the mode for numerical simulations. The total grid number reaches up to 2.38 million cells; the calculated cells were about 2.24 million. The minimum grid size is 0.25 cm in the z direction; the maximum grid size is 1 cm in any direction.

The boundary condition on the right-hand side of Block 2 was set as a steady volume rate current before it entered into Block 1. The discharge conditions in Block 2 for numerical simulation was equal to that used in physical experiments, as shown in Table 1.

As shown in Fig. 2(b), in Block 1, there is a bottom orifice and a left overflow weir. The boundary conditions of the free water surface, especially for the air core and overflow regions in the Flow-3D simulation were assumed at a specified pressure, an atmospheric pressure. The inter-block junction was at the right boundary of Block 1 and the left boundary of Block 2,

Table 2. Boundary conditions used in the numerical simulation.

Block 1 (The cylindrical chamber)		
Boundary	Location	Boundary Condition
Left side	x = 34 cm	Specified Pressure
Right side	x = 151 cm	Symmetry
Front side	y = 0 cm	Wall
Back side	y = 102 cm	Wall
Bottom plane	z = 0 cm	Specified Pressure
Top plane	z = 30.85 cm	Specified Pressure
Block 2 (The Inflow Channel)		
Left side	x = 151 cm	Symmetry
Right side	x = 250 cm	Volume flow rate
Front side	y = 80 cm	Wall
Back side	y = 102 cm	Wall
Bottom plane	z = 4.85 cm	Wall
Top plane	z = 30.85 cm	Specified Pressure

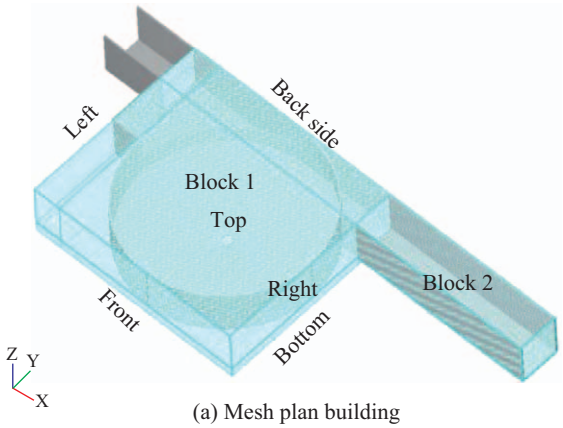

(a) Mesh plan building

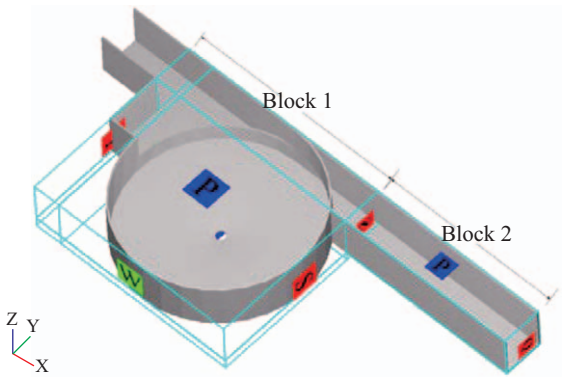

(b) Boundary condition setting

Fig. 2. Boundary conditions of VSB in FLOW-3D.

defined as the symmetrical condition. In addition, a no-slip condition was applied to wall boundaries. Furthermore, the whole process applied the centimeter-gram-second (CGS) unit system. The simulation continued until it reached a steady state condition. The boundary conditions for Blocks 1 and 2 were summarized in Table 2.

In FLOW-3D, there are five turbulence models available: the Prandtl's mixing length model, the one-equation, the two-equation k-epsilon RNG turbulence models, and a large eddy simulation (LES) model. In this investigation, the LES model was adopted. For the length scale, a geometric mean of the grid cell dimensions (Smagorinsky, 1963) was used herein,

$$L = \left(\delta x \delta y \delta z\right)^{1/3} \tag{1}$$

The scale of velocity fluctuations is obtained by the magnitude of L times the mean shear stress. These quantities are combined into the LES kinematic eddy viscosity, and this yields

$$\nu_T = \left(cL\right)^2 \times \sqrt{2e_{ij}\,2e_{ij}} \tag{2}$$

where ν_T is the turbulent kinematic viscosity, c is a constant having a typical value in the range of 0.1 to 0.2, and e_{ij} denotes the strain rate tensor components. This kinematic eddy viscosity incorporated with the dynamic viscosity as shown in Eq. (3) for turbulence flow was used throughout the FLOW-3D simulation.

$$\mu = \rho\left(\nu + \nu_T\right) \tag{3}$$

As shown in Fig. 3(a), the simulated velocity distributions at three selected depths were analyzed; these depths are h_z = 6.3 cm (the distance from the bottom), 10.3 cm, and 14.3 cm (near the surface layer), respectively. The velocity distributions in two sections, $\overline{AA'}$ and $\overline{BB'}$, in the radial direction as shown in Fig. 3(b) were discussed. The data points were selected along the radial direction at 0.5 cm interval in each section. There were totally 200 data points in each section.

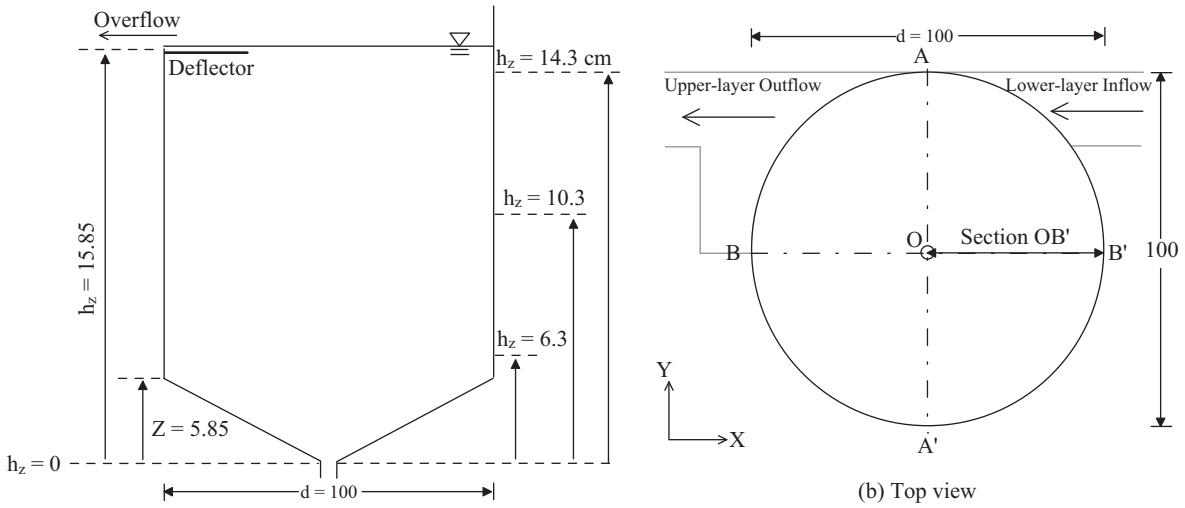

Fig. 3. Schematic diagram of a vortex settling basin used in this study.

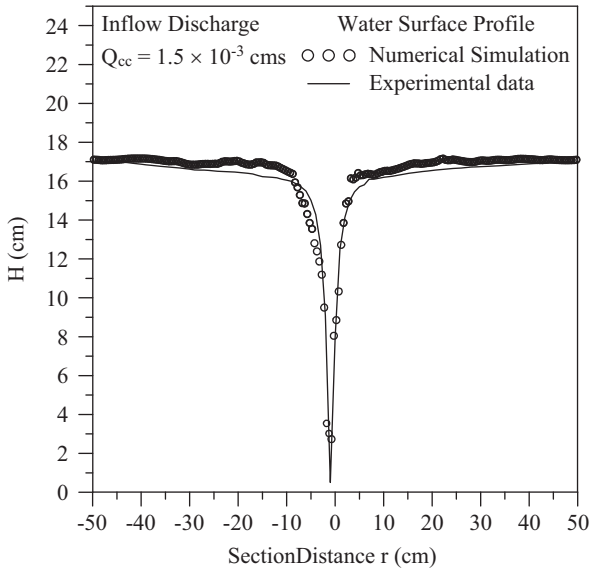

Fig. 4. Comparisons with water surface profiles obtained from numerical simulation and laboratory experiment in Section $\overline{BB'}$.

IV. RESULTS AND DISCUSSION

1. Verification of Numerical and Experimental Data

1) Water Surface Profiles

To confirm the FLOW-3D simulation results in the VSB, the water surfaces obtained from numerical simulation and experiment were compared, as shown in Fig. 4. The figure showed that the numerical and experimental surface profiles were very close to each other; the highest water surface in $\overline{BB'}$ section obtained from numerical simulation was 17.10 cm, which was 17.03 cm in section $\overline{OB'}$ of experimental data, and 19.95 cm in section $\overline{OB}$, respectively. The simulated surface profiles in the ranges of r = -30 cm to r = -10 cm and r = 10 cm to r = 30 cm are slightly higher than that of experimental results, with a difference up to 0.5 cm There was a slight left offset from the middle to the central location, and the water surfaces almost overlapped between r = -5 cm to r = 5 cm.

Concerning the location of the lowest point of the air core, we found that the numerical air core position fits the experimental result, particularly the center of the air core located at about 1 cm from the central in cross-section $\overline{\mathbf{BB'}}$. This offset phenomenon was caused by the tangential inflow. The lowest points of air-cores from experimental and numerical data fell on at (r = -1, h_z = 0.5) and at (r = -0.75, h_z = 2.73), respectively.

Regarding the size of the air core, the vortex air core region was determined by the slope of the water surface profiles. The zone having water surface slope larger than 0.05 was classified as a vortex air core. The results from numerical simulations showed that the air core was in the region between r = -12.75 cm and r = 14.75 cm, while it was found in the region between r = -12 cm and r = 13 cm for the results from experiments. They are quite close to each other.

Overall, the experimental results were more symmetrical than the numerical results. Except the small difference in the water surface profiles, the position of the air core center from numerical simulation is fairly consistent with that from the experiment.

2) Output Discharges

The outflow discharges obtained from the numerical simulations were also compared with those from experimental simulations, as shown in Fig. 5, in addition to the verification of the water surface profile. Under the condition that the orifice was kept at 3 cm, the results from three inflow discharges, such as Q_{cc} = 1.5 × 10^{-3} cms, 2.0 × 10^{-3} cms, and 2.5 × 10^{-3} cms, respectively, were used for comparisons. With this premise, the ex-

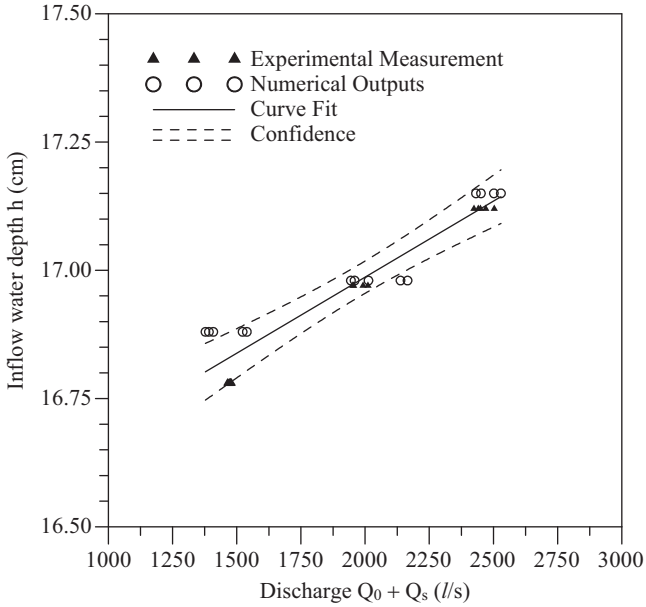

Fig. 5. Comparisons with inflow depth and outflow discharges of numerical simulation and experiment.

(a) Air core before the flow over the weir

(b) Air core in the small discharge

(c) Air core in the large discharge

(d) Air core floating in the cylinder chamber

Fig. 6. Air core forming process display.

perimental and numerical data were drawn in Fig. 5 with the inflow water depths and the outflow discharges. Fig. 5 shows that, in the case of $Q_{cc} = 1.5 \times 10^{-3}$ cms, the variance of inflow water depth is within 0.1cm, while the numerical outflow discharge is less stable, tending to a little float up and down on the default flow. For $Q_{cc} = 2.0 \times 10^{-3}$ cms, the variance of the two water depths is within 0.01cm, but the simulated outflow discharge has a little float-up and down variation. Lastly, for $Q_{cc} = 2.5 \times 10^{-3}$ cms, the variance of the inflow depth is within 0.03 cm, and the discharges are more close to each other. The analysis diagram signifies that with the discharge increasing, the values of experimental and numerical simulation become closer to each other. It is also shown that the outflow of numerical simulation at larger discharge is steadier than that at smaller discharge, with the outflow discharge getting closer to the default inflow discharge. The experimental inflow is controlled by an electronic flow meter which has an error around 1%. The discharge discrepancy from numerical simulations is only up to 3.46%, and it implies that the numerical results are acceptable.

2. Air Core Forming Process

During the process of vortex development in the VSB from the starting point to the steady condition requires more attention. Whether the vortex is suitable or not, it should be judged from the state of steadiness in the swirling process, the spiral line of the water surface profile of the air core, and the size of the air core.

When the flow entered the cylinder chamber by the tangential direction, the flow started the circular motion until the water reached over the height of the overflow weir, as shown in Fig. 6(a). At that moment, the vortex represented a symmetrical form; and, the surface profile showed a smooth curve as well.

After the water level exceeded the overflow weir, the vortex was impacted. The whole vortex had a little offset to the overflow weir, with the offset degree proportional to the inflow quantity. Fig. 6(b) and Fig. 6(c) are the results of inflows $Q_{cc} = 1.5 \times 10^{-3}$ cms and $Q_{cc} = 2.5 \times 10^{-3}$ cms, respectively. When the inflow was smaller, the shape of the air core became a slender-type without much deformation, as Fig. 6(b) shows. However, by gradually increasing the inflow, the size of the air core became wider, and it started to generate a spiral surface profile that circled the vortex, as shown in Fig. 6(c). Once the inflow kept on increasing, and was influenced by the raising tangential velocity, the air core with spiral line would start to swing.

When the tangential velocity of the inflow exceeded the limit

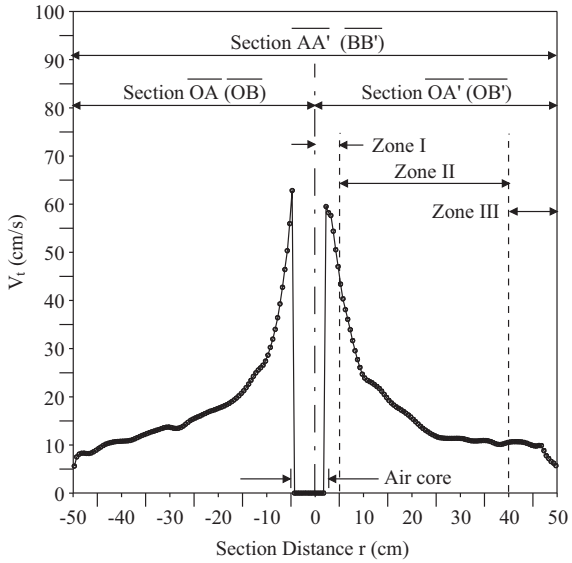

Fig. 7. Description of the cross-section location. Zone I: the high velocity area (0 ≦ r ≦ 0.1R), Zone II: the transition zone (0.1 ≦ r ≦ 0.8R), Zone III: the wall zone (0.8 ≦ r ≦ 1R).

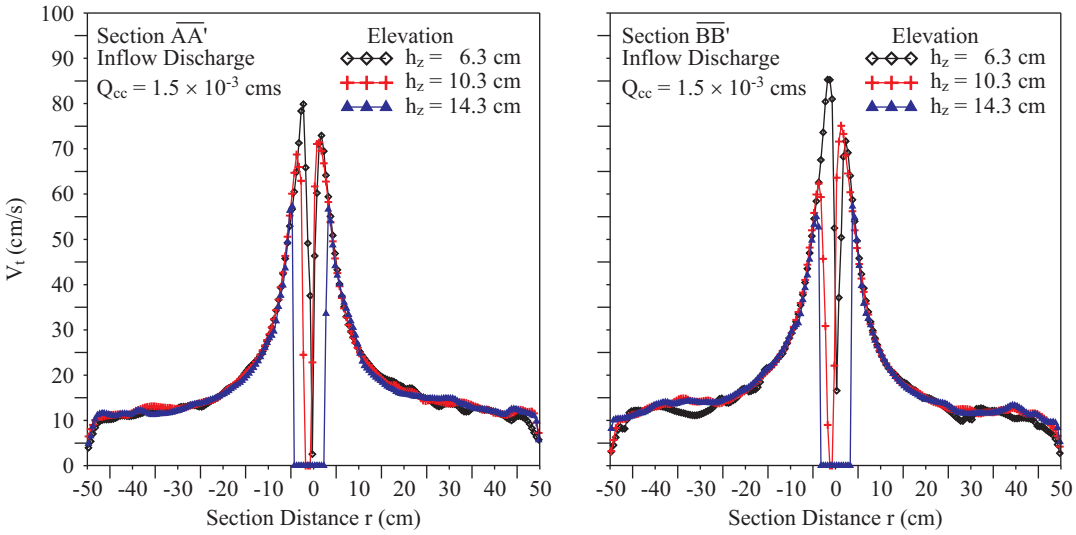

Fig. 8. Tangential velocity distributions at three different elevations under a specified inflow discharge.

of the circular motion, the air core would change from Figs. 6(c) and (d). As a result, the sharp point at the bottom would raise upwards and become shorter due to the over far distance of the orifice going astray from the center. Once the inflow quantity remained the same, the air core would have such shape floating in the cylinder chamber. In addition, when the air core raised in a moment, the overall velocity in the VSB would be changed, particularly the axis speed would generate the positive axis velocity component. From the perspective of sediment removal, this phenomenon is not a suitable vortex.

Nevertheless, the vortex itself is a very complicated issue along with many influential factors from the VSB, such as the height of the overflow weir, the orifice size, horizontal deflector, the vortex chamber slope, and so on. All of these factors could affect the vortex's steadiness and intensity in a certain degree.

3. Comparisons of Velocities

In the following paragraphs, we discuss three velocity components, tangential velocity V_t, redial velocity V_r, and axial velocity V_z respectively. As shown in the explanatory diagram of Fig. 7, the cross-sections $\overline{OA}$ and $\overline{OB}$ are on the left side of the diagram and cross-sections $\overline{OA'}$ and $\overline{OB'}$ are on the right side of the diagram. The air core is located in the middle of the diagram.

1) Tangential Velocities

Fig. 8 shows the tangential velocity profiles at three different elevations under a specific inflow discharge. Impacted by the

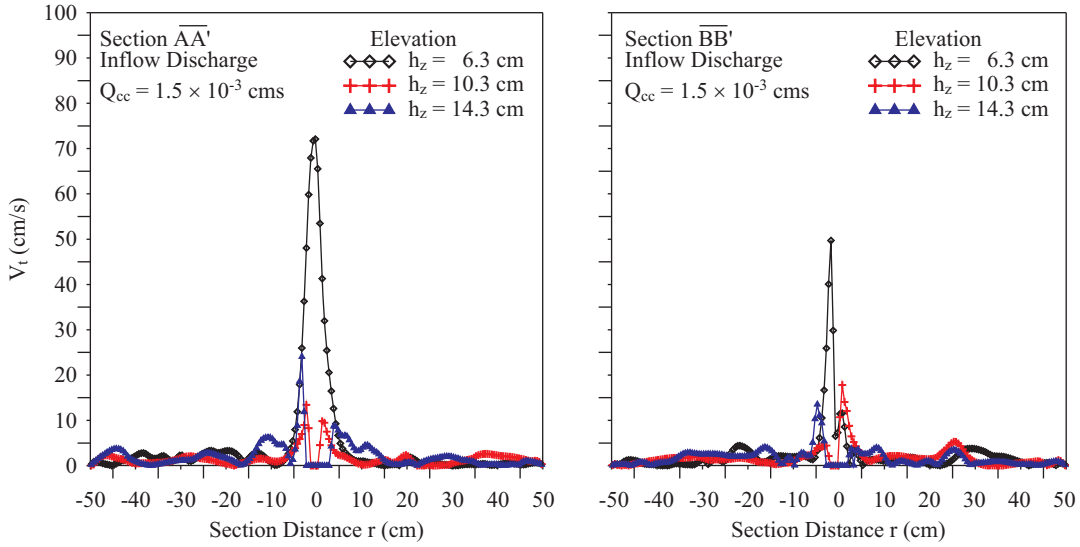

Fig. 9. Radial velocity distribution at three different elevations under a specified inflow discharge.

tangential direction of the inflow, the tangential velocity becomes the largest of the three velocity components. Also, it is an important factor for maintaining a continuous circular motion of the currents. The tangential velocity distribution presented that the inner part is similar to a free vortex, while the outer part is similar to a forced vortex, and this phenomenon is consistent with the literature proposed by Rankine. Afterwards, such vortex is called "Rankine-Vortex".

The tangential inflow caused a little offset phenomenon of the vortex center, resulting in the flow field in the circulation chamber that is not completely stable. Due to the inflow direction, it could be seen that the tangential velocity from the section $\overline{OA}$ at the entrance to the middle section $\overline{OA'}$ showed a gradual increase. But, because of the currents in the section B' had returned to the entrance, the velocity returned with the inflow speed as the vicinity of the flow velocity. The tangential flow velocity would influence the removal efficiency of sediment if having in the chamber. Regardless of the water depth, the velocity rapidly rose with the direction of the wall to the orifice. Particularly, when the distance to orifice was $0.1 \leqq r \leqq 0.8R$ (the transition zone, Zone II), the flow velocity in this range increased many times with the direction of the wall to the orifice. The largest velocity in Zone II could even reach 8-10 times more than that at the entrance's flow velocity. In the range of $0 \leqq r \leqq 0.1R$, called Zone I, it is a high flow velocity area. On the other hand, there is a lower velocity zone at the wall boundary of $0.8 \leqq r \leqq 1R$. The low velocity zone is called Zone III.

The figure also shows that the tangential velocity distributions at the three different water depths were quite similar in Zones 2 and 3. In the high speed zone, the tangential velocity tended to increase a little with the depth. The air core was in a tapered shape, wider at the top and narrow at the lower part. No water existed in the vortex air core here. Some zero points appeared on the graph in the air core area, especially at z = 14.3 cm.

2) Radial Velocities

Radial velocity in a VSB controls the mechanism of sediment that moves to the bottom orifice. In zone II and zone III, regardless of the water depth, the radial velocity variation is not obvious, as shown in Fig. 9. In Zone I, near the VSB bottom, at $h_z = 6.3$cm, the radial velocity significantly increases; and, this phenomena will be beneficial to sediment removal.

3) Axial Velocities

The sediment is removed through the bottom orifice mainly according to the axial velocity. As shown in Fig. 10, the axial velocity fluctuates between the positive and the negative at the cross-section $\overline{OA}$ and the cross-section $\overline{OB}$ at $r = \pm 0.5R$. This phenomenon, caused by the inflow from the cross-section $\overline{OA}$, matched with the results of the laboratory observations. Although the influence of the inflow tangential force was larger in the beginning, the tangential force gradually became smaller during the movement. In addition, the water flowed through the overflow weir and was close to the inflow, so the flow in the cross-section $\overline{OA'}$ and cross-section $\overline{OB'}$ showed a relatively unstable state, leading to the fluctuation.

In Zone I, we can easily see that the velocity increased rapidly and the deeper the water, the more the negative velocity. In general, the axial velocity at the circulation chamber with a flushing orifice shall all be downward, which is displayed as the negative value in this study. Nevertheless, influenced by the overflow weir and the vortex offset, the vortex cannot fully touch the orifice, making it easy to result in the oscillation phenomenon shown in Fig. 6(d). When the vortex touches the bottom orifice, the air core directly gets connected to the orifice. On the other side, when the vortex was not in the center, the offset of the air core could cause the separation from the orifice. Therefore, the tip of the air core would be lifted and resulted in

Table 3. Velocity variations between the water before and after the water overflowing in high velocity zone, transition zone and wall zone.

		V_t (cm/s)		V_r (cm/s)		V_z (cm/s)	
		Before overflow	After overflow	Before overflow	After overflow	Before overflow	After overflow
Zone I	h_z = 6.3 cm	60.2	57.5	24.0	27.0	**-6.4**	**-6.5**
	h_z = 10.3 cm	60.4	52.4	12.4	24.0	**-1.1**	**-3.1**
	h_z = 14.3 cm	52.6	51.2	12.0	11.9	5.3	2.1
Zone II	h_z = 6.3 cm	27.0	20.2	2.3	2.0	0.2	0.2
	h_z = 10.3 cm	27.1	20.2	2.4	1.7	0.1	0.1
	h_z = 14.3 cm	26.8	20.1	2.8	2.0	0.4	0.1
Zone III	h_z = 6.3 cm	16.6	12.1	1.1	0.8	**-0.2**	**-0.2**
	h_z = 10.3 cm	17.4	12.6	1.5	0.8	0.4	0.0
	h_z = 14.3 cm	17.2	12.0	1.4	1.2	0.5	0.2

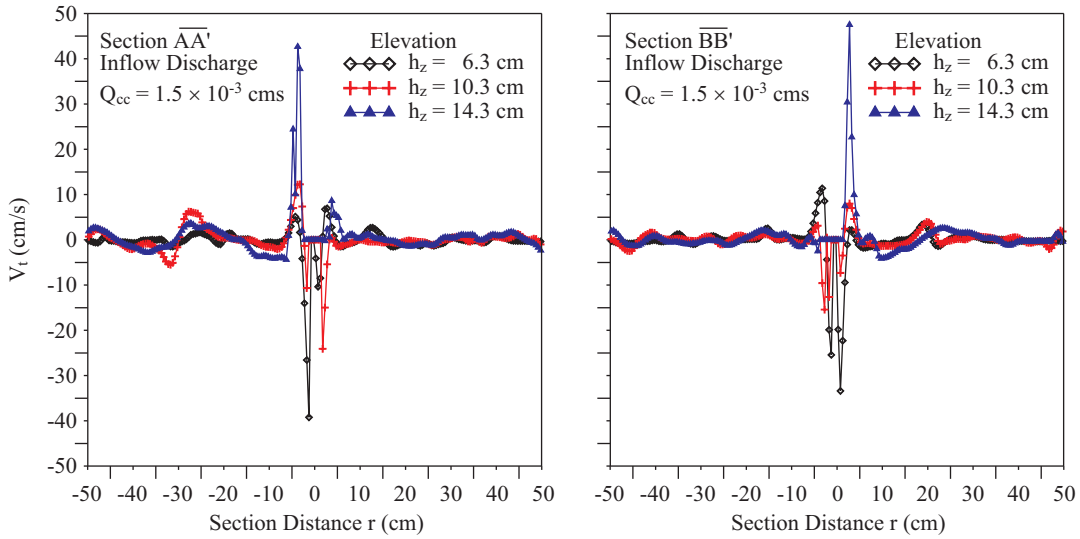

Fig. 10. Axial velocity distribution at three different elevations under a specified inflow discharge.

upward axial velocity. Thus, the result has shown a positive value in the analysis diagram. Regardless of the positive or negative value, the minimum axial velocity is 0 cm/s and the maximum one 50 cm/s. These indicate that the motion trajectory of the particle will be close to the horizontal circular motion in zone II and zone III, and a strong vertical motion in zone I. Fig. 10 shows that the area close to the bottom orifice has a larger negative axis velocity that is beneficial to sediment extraction from the bottom orifice.

4. Velocity Profile Variations

The velocity profiles of each velocity component of the vortex flow with and without overflow were also compared as shown in Fig. 11. From r = 0.2R to zone III, the tangential velocities with (after) overflow were smaller than those without (before) overflow, with a decrease of tangential velocity about 25%-30%. However, there was a relatively smaller change in Zone I. There were some points with velocity zero in the center, which means the data were located in the air core, and this showed that the air core without water overflow was somehow wider than that with overflow.

As shown in Figs. 11(d)-(f), there are no significant variations in radial velocities in Zones II and III. The radial velocity rises obviously after water overflowed in Zone I, especially at depth h_z = 6.3 cm. The closer to the water surface, the more consistent the radial velocity, as shown in Fig. 11(f).

Figs. 11(g)-(i) show the comparisons of the results of axial velocities. The positive values signify upper directions, and negative values down directions. These figures show that the changes in axial velocities along the radial direction in Zones II and III are not large (within ±5 cm/s). Nevertheless, in Zone I, the values swung up and down extensively. No matter it was before or after water overflowed, the axial velocity was towards the orifice. A greater number of positive values closer to water surface show that when the particles were closer to the surface of the vortex, it was not beneficial for them to sink downwards. This could be a reason to design a VSB with a culvert intake passage entry. For comparison, the velocity data

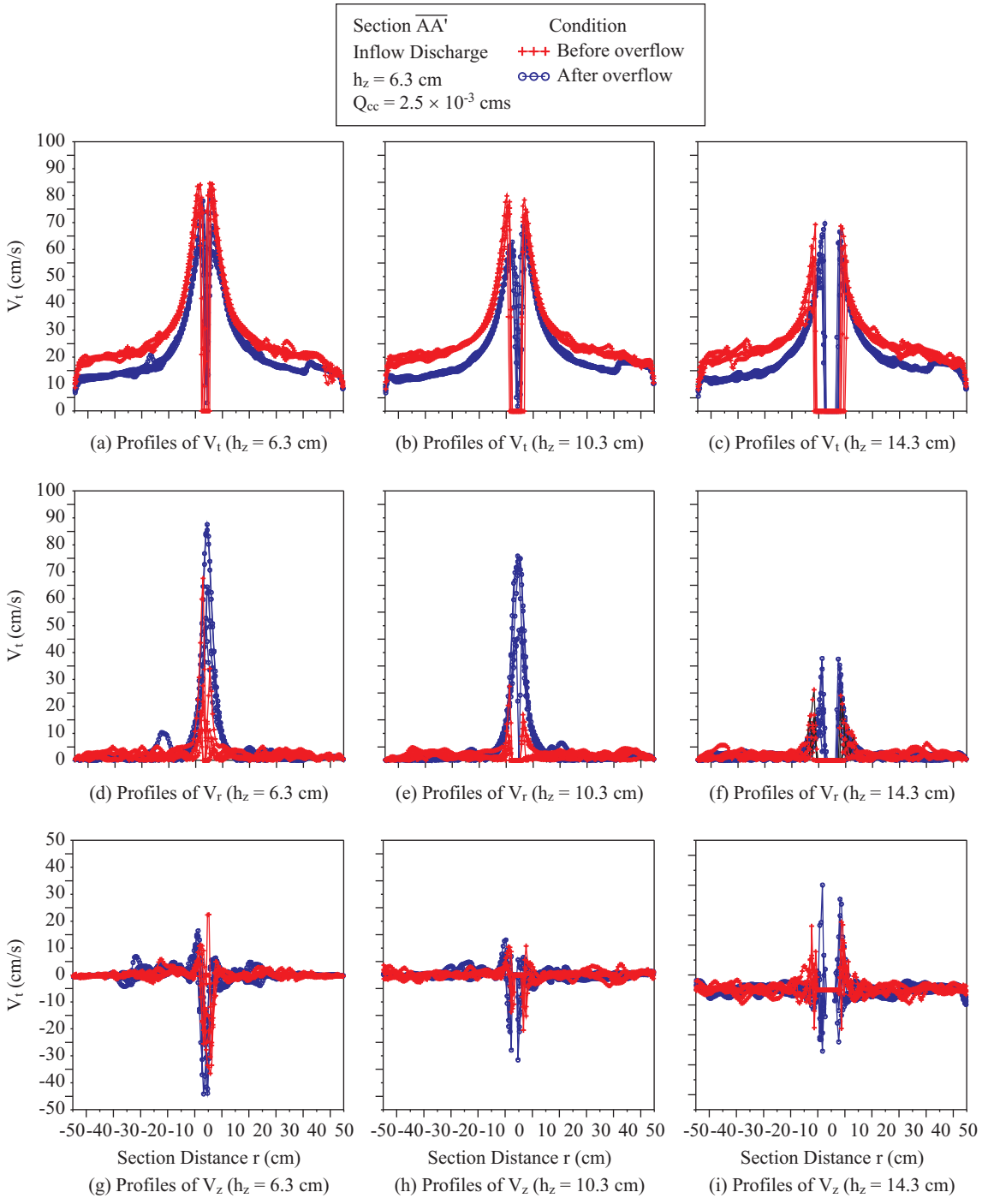

Fig. 11. Velocity profile comparisons for vortex flow with and without overflow at the water depth h_z = 6.3 cm, 10.3 cm, 14.3 cm. (a)-(c): tangential velocity profiles; (d)-(f): radial velocity profiles; (g)-(i): axial velocity profiles.

before and after water overflowed are shown in Table 3.

5. Oscillation of Air Core

The stability of vortex motion in a VSB is an important factor in the efficiency of sediment removal. In this section, the vertical motion of vortex is classified into three phenomena for discussion; i.e., the air core leaves the orifice and shortens, the shape of air core remains unchanged, and the bottom end of air core extends downwards to connect the flushing orifice. The average velocities of three kinds of instantly changing forms were analyzed by using the 50 seconds of simulation for the three respectively. Among the simulations, there are 18 seconds of the air core leaving the orifice and shortening, 13 seconds of the shape remaining unchanged and 19 seconds of

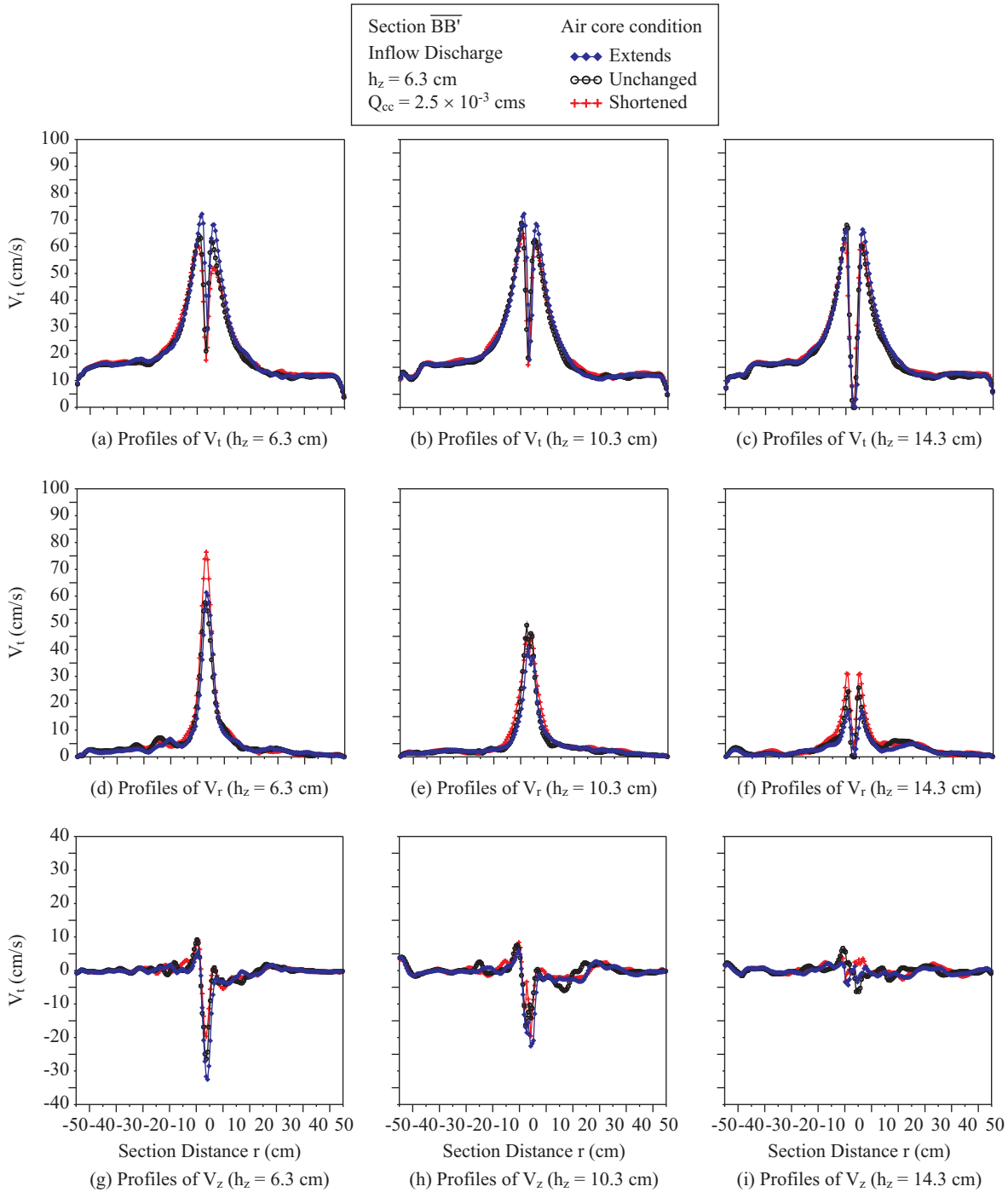

Fig. 12. Velocity profile analyzing in three kinds of air core phenomenon during certain period of time at the water depth h_z = 6.3 cm, 10.3 cm, 14.3 cm. (a)-(c): tangential velocity profiles; (d)-(f): radial velocity profiles; (g)-(i): axial velocity profiles.

the air core extending downwards to connect the flushing orifice. As shown in Fig. 12(a), outside the high-velocity zone, when the air core is extending downwards, the tangential velocity averaged in a long time remains unchanged either in depth h_z = 6.3 cm, 10.3 cm or 14.3 cm. In Zone I, when the air core is extending downwards, the tangential component is apparently higher than it was in the other two cases.

In addition, the radial velocity in Zone I is significantly smaller with increasing water depth. The radial velocity is also increasing in cases when the air core becomes short. The shorter air core caused the wider of the water cross section and more water flowing out through the bottom office, thus increasing the radial velocity. In Zone I, a significantly greater negative axial velocity is produced when the air core extending downward.

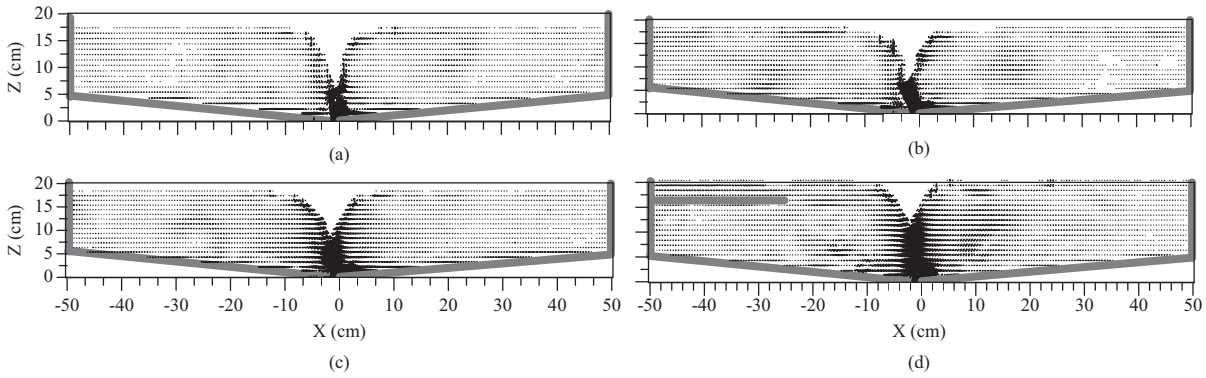

Fig. 13. Computed velocity vectors under different situation of air core. (a) $Q_{cc} = 1.5 \times 10^{-3}$ cms, no horizontal deflector (b) $Q_{cc} = 2.5 \times 10^{-3}$ cms, no horizontal deflector, (c) $Q_{cc} = 4.0 \times 10^{-3}$ cms, no horizontal deflector, (d) $Q_{cc} = 2.5 \times 10^{-3}$ cms, with a horizontal deflector.

The shorter air core has smaller negative axial velocity. This phenomenon is not the vortex type we expected. In that we can assume that the shortened air core causes the small tangential velocity, large radial velocity and small negative value of axial velocity. The key factors on air core oscillation are the tangential inflow velocity and the size of bottom orifice. The oscillation of air core may cause some changes in the flow field, especially in the high velocity zone, but the overall change in the whole flow field is not so obvious.

6. Flow Field Characteristics

Figs. 13(a)-(d) are flow field vector graphs. Complexity of vortex structures itself and the influence of VSB design have led to even more complex structure of internal vortex of VSB. Figs. 13(a)-(c) are the three cases for the inflow discharge $Q_{cc} = 1.5 \times 10^{-3}$ cms, 2.5×10^{-3} cms, and 4×10^{-3} cms, respectively, without the installation of a horizontal deflector in the VSB. Fig. 13(d) is the result of $Q_{cc} = 2.5 \times 10^{-3}$ cms with a horizontal deflector in the VSB. In the physical model experiment, although some variations in the flow field can be seen by the naked eyes, the process cannot be converted into images for illustration. Therefore, this study illustrates it by the analysis of velocity vectors The fields were not consistent everywhere in the VSB, because different impacts would be generated by different factors like inflow positions, angles, structure design, and so on.

For example, in Fig. 13(a), at $Q_{cc} = 1.5 \times 10^{-3}$ cms, in the view of the whole vector graph, except some bigger vectors surrounding the air core and the bottom, the velocity vectors were more uniform. After increasing the discharge up to $Q_{cc} = 2.5 \times 10^{-3}$ cms, clockwise vortex appeared at the right hand side of the vector figure, while another similar flow field appeared at the corresponding position at the left hand side. To increase the inflow discharge up to $Q_{cc} = 4.0 \times 10^{-3}$ cms, then, the counterclockwise flow field at the left hand side became more apparent than it was at the flow of $Q_{cc} = 2.5 \times 10^{-3}$ cms, while the clockwise flow field at the right hand side disappeared. As for the surrounding area of the air core, the velocity vectors at the case of $Q_{cc} = 4.0 \times 10^{-3}$ cms were larger than those at the case of $Q_{cc} = 2.5 \times 10^{-3}$ cms. In the abovementioned figures, without the installation of a horizontal deflector, they showed that the velocity vectors in the area near the side walls were weaker in the whole device.

As shown in Fig. 13(d), after the horizontal deflector was inserted in the VSB, the intensity of vector in the flow field was stronger than without the deflector, and the flow under the horizontal deflector became more uniform. To view from the tendency that the velocity vector graph became stronger, and a curve of air core was formed from the flushing orifice to the top of the horizontal deflector. Therefore there appears to be a correlation with the horizontal deflector. The vector graphs cannot represent the flow fields in such a status, but we can generalize several points by observing the vector graphs at certain times.

The flow fields in the VSB changes with time, the intensity of the flow field surrounding the air core increased with the flow, and the position at r = 0.25R from the center tended to produce the clockwise and the anticlockwise vortex. Close to the bottom was a layer of a strong intensity of vector in which the direction of velocity vectors pointed to the flow in the flushing orifice, having a potential to bring sediment into the flushing orifice.

The installation of a horizontal deflector in the VSB results in the increase of residence time for the particles in the basin, and has certain effects to raise the flow velocity. Without the horizontal deflector, in spite of the inflow entering the vortex basin from a culvert, due to the inflow is directly opposite to the overflow weir, part of water flow could directly overflow through the weir before it makes a circular motion in the basin. In such case, it is unfavorable for removing the particles. On the contrary, with the installation of a horizontal deflector, inflow could be restricted to flow in the vortex basin, even in the low velocity zone or area close to the side wall. However, as long as it is possible to sink to the bottom layer or enter the high velocity zone, the particles could be removed.

V. CONCLUSION

This paper briefly summarized the development of a vortex settling basin (VSB) by previous researchers, including direct measurements and numerical simulations. Using FLOW-3D, this study numerically assessed the velocity distribution in a

VSB, having a cylinder of 100 cm in diameter and 30 cm in height. The vortex characteristics were successfully simulated by using Flow-3D with turbulence model of LES. It can be concluded that numerical simulation is an efficient tool in analyzing free surface of VSB. Comparison of experimental and numerical simulated results shows that Flow-3D can perform a very much alike appearance of the VSB vortex appearance. Moreover, the offset location of the vortex center and the size of the air core were presented within a relative small error range.

The characteristics of velocity components (tangential, radial, and axial velocities) at these three depths have been discussed in this study. The velocity of tangential inflow is a key factor leading to the offset of air core center. The tangential velocity rapidly rises along the direction from the side wall to the center axis. The radial velocity increases with the water going to deeper inside the high velocity area. The area close to the bottom orifice has a larger negative axis velocity that is beneficial to sediment extraction from the bottom orifice. The oscillation of air core might cause the flow field changes, especially in the high velocity zone, but the overall change in the whole flow field is not obvious. In addition, the installation of a horizontal deflector not only increase the residence time of particle but also raise the tangential flow velocity in the VSB.

Even though this study has conducted a good simulation on the flow field in a VSB by using Flow-3D, it is noted that any change in the design of VSB could cause significant effects on the flow field in the VSB due to its extremely complex flow characteristics. Therefore, continued investigations are needed so as to get more a better understanding on the flow field in a VSB under different design conditions.

REFERENCES

Athar, M., U. C. Kothyari and R. J. Garde (2002). Sediment removal efficiency of vortex chamber type sediment extractor. Journal of Hydraulic Engineering, ASCE 128(12), 1051-1059.

Cecen, K. and N. Akmandor (1973). Circular settling basins with horizontal floor. MAG Report No 183, TETAK, Ankara, Turkey.

Chapokpour, J. and J. Farhoudi (2011). Turbulent flow measurement in vortex settling basin. Iranica Journal of Energy & Environment 2(4), 382-389.

Chapokpour, J., F. Ghasemzadeh and J. Farhoudi (2012). The numerical investigation on vortex flow behavior using FLOW-3D. Iranica Journal of Energy & Environment 3(1), 88-96.

Flow Sciences Incorporated (2011). Flow-3D user manual version 10.0.

Hajiahmadi, A., M. Saneie and M. A. Moghadam (2014). Effects of curvature submerge vane in efficiency of vortex settling basin. Journal of Applied Research in Water and Wastewater 1(2), 80-85.

Hite, E. J. Jr. and W. C. Mih (1994). Velocity of air-core vortices at hydraulic intakes. Journal of Hydraulic Engineering, ASCE 120(3), 284-297.

Hsu, Y. C., C. Y. Yang and C. D. Jan (2013). Experimental study on the effect of inflow sediment concentration on sediment removal efficiency of a deep-depth vortex chamber type sediment extractor. Proceedings of the 35th International Association for Hydro-Environment Engineering and Research World Congress, Chengdu, China, 11525.

Jan, C. D., Y. C. Hsu and T. S. Huang (2014). Experimental study on the effect of a diversion pier on stabilizing the vortex flow in a vortex-chamber-type sediment extractor. Taiwan Water Conservancy 62(1), 44-55. (in Chinese, with English Abstract)

Keshavarzi, A. R. and A. R. Gheisi (2006). Trap efficiency of vortex settling chamber for exclusion of fine suspended sediment particles in irrigation canals. Journal of Irrigation and Drainage Engineering 55, 419-434.

Mashauri, D. A. (1986). Modeling of vortex settling chamber for primary clarification of water. Ph.D. Thesis, Tampere University of Technology, Tampere, Finland, published.

Niknia N., A. R. Keshavarzi and E. Z. Hosseinipour (2011). Improvement the trap efficiency of vortex chamber for exclusion of suspended sediment in diverted water. Proceedings of World Environmental and Water Resources Congress, Palm Springs, California, USA, 4124-4134.

Noguchi, T., S. Yukimoto, R. Kimura and H. Niino (2003). Structure and instability of a sink vortex. Proceedings of the 4th Pacific Symposium on Flow Visualization and Image Processing, Chamonix, France, F4080.

Paul, T. C., S. K. Sayal, V. S. Sakhanja and G. S. Dhillon (1991). Vortex settling chamber design considerations. Journal of Hydraulic Engineering, ASCE 117(2), 172-189.

Smagorinsky, J. (1963). General circulation experiments with the primitive equations. Monthly Weather Review 91(3), 99-164.

Wang, S. J., Z. Zhou, J. Hou and X. Y. Qiu (2002). Flow field characteristics of the sand funnel and its mechanics of sediment transport. Journal of Hydrodynamics Ser. B, 3, 130-134.

Ziaei, A. N. and J. M. McDonough (2007). Using vorticity to define conditions at multiple open boundaries for simulating flow in a simplified vortex settling basin. International Journal for Numerical Methods in Fluids 54, 1-28.